05,08

Configurations of higher-order magnetic skyrmions and a Pearl vortex in a bound state

© A.D. Fedoseev[1], M.S. Shustin[2,¶], D.M. Dzebisashvili[1]

[1] Kirensky Institute of Physics, Federal Research Center KSC SB, Russian Academy of Sciences, Krasnoyarsk, Russia
[2] L.D. Landau Institute for Theoretical Physics, Chernogolovka, Russia

¶ E-mail: mshustin@yandex.ru

Received March 6, 2025
Revised March 6, 2025
Accepted May 5, 2025

Within the framework of the magnetic energy functional of the hybrid 2D structure superconductor-chiral magnet, which takes into account: exchange interaction, single-ion anisotropy, as well as orbital and Zeeman effects of the Pearl vortex scattering fields, the stabilization conditions of higher-order magnetic skyrmions with topological charges $|Q| = 3, 4$ are studied. In contrast to the case of $|Q| = 2$, studied earlier [JETP Letters **120**, 539–546 (2024)], skyrmions with higher $|Q|$ do not necessarily form non-axial configurations of a bound pair with a Pearl vortex. Moreover, for skyrmions with $|Q| = 3$, the competition of interactions in the continuum limit allows for different degrees of coaxiality, however, the coaxial configuration cannot be stabilized on a real discrete lattice due to the small size of the skyrmions. Skyrmions with $|Q| = 4$ form stable coaxial pairs with a Pearl vortex.

Keywords: magnetic skyrmions, Pearl vortex.

DOI: 10.61011/PSS.2025.07.61886.20HH-25

1. Introduction

Two-dimensional magnetic skyrmions (MS) are localized vortex-like configurations for which the magnetization field $\mathbf{m}(\mathbf{r})$ belongs to a nontrivial component of the homotopy group $\pi_2(\mathbb{S}^2) \in \mathbb{Z}$ [1,2]. Since the configuration for the ferromagnetic state corresponds to a trivial component, a smooth collapse of the MS cannot be realized without overcoming the energy barrier. The latter underlies to the practical interest in the study of MS as potential objects for the implementation of the element base of magnetic memory devices, spintronics and superconducting electronics [3–5].

A quantitative characteristic that makes it possible to determine whether MS belongs to certain homotopy classes is the topological charge Q, defined in terms of the magnetization field as [1,2]:

$$Q = \frac{1}{4\pi} \int\limits_{\mathbb{R}^2} \left(\mathbf{m} \cdot \left[\frac{\partial \mathbf{m}}{\partial x} \times \frac{\partial \mathbf{m}}{\partial y} \right] \right) d^2\mathbf{r}, \qquad (1)$$

The most studied are skyrmions with $|Q| = 1$, however, in recent years, studies of more exotic MS with different values of Q have significantly intensified, namely: higher-order skyrmions [6,7], skyrmion bags [8–12], biscyrmions [13], and so on. Among the noted structures, higher-order magnetic skyrmions (HOMS) are vortices whose magnetization field can be parameterized in terms of the skyrmion angle $\Theta(r)$ as:

$$m_x = \sin\Theta(r)\cos n\varphi;$$
$$m_y = \sin\Theta(r)\sin n\varphi; \quad m_z = \cos\Theta(r). \qquad (2)$$

Here r and φ are radial and angular variables of the polar coordinate system on the film with the origin coinciding with the center of the skyrmion; n is the vorticity of the HOMS related with the topological charge by the ratio $n = -Q$. Thus, HOMS with different values of n belong to different homotopy classes, are metastable configurations, and cannot transform into each other without overcoming the energy barrier — the greater the larger the size of HOMS.

The chiral Dzyaloshinskii–Moriya interaction (D–M) is most actively studied among the mechanisms of stabilization of magnetic skyrmions [14]. However, in the case of HOMS with $|n| > 1$, the latter makes a zero contribution to the magnetic energy functional. In addition to the D–M interaction, other mechanisms were considered, caused, for example, by the magnetostatic interactions [7,15], frustrated exchange links [6,16] or hybridization of localized magnetic moments with collectivized electrons [13,17]. An analytical profiles was also proposed for a system of several magnetic vortices, including those carrying a topological charge $|Q| > 1$, in planar nanostructures with an arbitrary boundary shape [18].

Recently, the authors proposed an additional mechanism for the stabilization of HOMS with $|n| > 1$ due to the orbital effects of inhomogeneous magnetic fields [19–21]. As the latter, we considered the stray fields of the Pearl vortex (PV). In the case of coaxial configurations with coincident coordinates of the centers of the HOMS and the Pearl vortex, an analytical theory of bound states was developed and it was demonstrated that for strongly correlated systems, the contribution of the orbital terms to the energy of the

HOMS can be comparable to the contribution from the D−M interaction [19,20]. Later, it was shown [21] that orbital effects allow for the stabilization of non-coaxial configurations by analogy with the case of coupled pairs of PV−MS with $|Q| = 1$ (stabilized by the D−M interaction), studied in detail in a series of recent papers [22–25]. It has been shown that non-coaxial coupled configurations of the PV−HOMS are always appear in the simplest case $n = 2$ [20].

On the other hand, a qualitative analysis of the Zeeman and orbital contributions to the magnetic functional, partially carried out in Ref. [21], shows that HOMS with $n > 2$ can potentially form coaxial configurations. The latter, in turn, can become a platform for the implementation of Majorana bound states on magnetic skyrmions [26–31]. This paper studies the conditions for stabilization of coupled pairs of PV−HOMS with $n > 2$ due to the orbital effects of PV stray fields and shows the possibility of implementing coaxial bound states.

2. HOMS energy functional in the Pearl vortex scattering field

We will consider the conditions for the formation of HOMS in hybrid two-dimensional superconductor/ferromagnetic structures within the framework of the following classical magnetic functional on a triangular lattice:

$$\mathscr{H} = -\sum_{\langle f,g\rangle} \mathscr{J}\cdot \mathbf{S}_f \cdot \mathbf{S}_g + \sum_{\langle f,g,l\rangle\in\Delta} \mathscr{K}\cdot \mathbf{S}_f \cdot [\mathbf{S}_g \times \mathbf{S}_l] - \mathscr{B}\sum_f S_f^z - \mathscr{A}\sum_f (S_f^z)^2 \quad (3)$$

Here $\mathbf{S}_f$ are classical three-component vectors on the site f. The first term of the right side (3) describes the exchange interaction of the ferromagnetic type, $\mathscr{J} > 0$, between neighboring sites f and g. The second term describes the three-spin interaction between the three nearest sites f, g and l, forming a minimal plaque Δ on a triangular lattice. It is also called scalar chiral interaction (SCI). The parameter $\mathscr{A} > 0$ describes a single-ion anisotropy of the type „easy axis“, $\mathscr{B}$ is the strength of an external magnetic field expressed in energy units directed along the quantization axis z perpendicular to the film.

A spin Hamiltonian of type (3) can be obtained by considering effective interactions in two-dimensional Mott-Hubbard insulators [19,32,33]. In this case, the term $\propto \mathscr{J}$ has the meaning of a superexchange interaction, and the terms $\propto \mathscr{K}$ and $\propto \mathscr{B}$ describe the orbital and Zeeman effects of an external magnetic field, respectively. In this case, the inhomogeneous amplitude $\mathscr{K}(f, g, l)$ is determined by the magnetic flux Φ_Δ through the triangular plaquet Δ. The term with easy axis anisotropy $\propto A$ can be caused both by crystal field effects and effectively induced by dipole−dipole interactions for skyrmions of sufficiently large spatial dimensions [22,34,35]. It has been shown that in the regime of strong electronic correlations, a hierarchy of effective interaction amplitudes is realized, $\mathscr{J} \gg \mathscr{K} \gg \mathscr{A}$, which we will continue to adhere to.

When describing the Pearl vortex, we will assume that the parameter of its effective length λ significantly exceeds the characteristic sizes of the skyrmion. Accordingly, when describing the interaction between superconducting and magnetic vortices, we will take into account only the influence of the former on the latter, ignoring the reverse influence. We also neglect the superconducting proximity effect, considering that PV acts on magnetic skyrmions only through inhomogeneous stray fields: $\mathbf{H}(\rho, \varphi, z \to 0_+) = H_z(\rho)\cdot \mathbf{e}_z + H_\rho(\rho)\cdot \mathbf{e}_\rho$. Hereafter, $\rho = [(x - x_0)^2 + (y - y_0)^2]^{1/2}$ is used to denote a radial variable of the polar coordinate system with the origin coinciding with the center of the Pearl vortex, $(x_0, y_0) = -(a\cdot\cos\phi_0, a\cdot\sin\phi_0)$ (see Figure 1). The radial dependence of the components $H_{z/\rho}$ is determined by the expressions [25,36–38]:

$$H_{z/\rho}(\rho) = \frac{s_H\Phi_0}{2\pi}\int_0^\infty \frac{qJ_{0,1}(q\rho)}{1 + 2q\lambda}\,dq \cong \frac{s_H\Phi_0}{4\pi\lambda}\frac{1}{\rho}, \quad (4)$$

where the multiplier $s_H = \pm 1$ determines the mutual directions of the vortex field and the saturation magnetization of the film, Φ_0 is the quantum of the magnetic flux. When writing (4) we assumed that the sizes of the vortex core ξ are negligible compared to the characteristic sizes of the skyrmion and the Pearl vortex.

We will consider the issue of stabilization of the HOMS in an inhomogeneous field within the framework of a variational approach for the continuum version of the classical functional (3). We will consider a two-parameter ansatz of the skyrmion angle as a trial function describing the formation of the HOMS [39]:

$$\Theta(r, R, w) = 2\arctan\left(\frac{\cosh R/w}{\sinh r/w}\right). \quad (5)$$

Such parametrization, together with (2), makes sense of an axially symmetric 1D domain wall, where w is its width, R is the distance from the center of the skyrmion to its middle. All distances are measured in units of the lattice parameter. Next, we will assume that the centers of the PV and the HOMS can be shifted relative to each other, and their relative position is parameterized by the polar variables — the distance $a \ll \lambda$ between the centers and the angle φ_0. The visualization of the spatial profile of the HOMS with $n = 2$, constructed using (2) and (5), as well as the geometry of the relative position of the HOMS and PV are shown in Figure 1. It is important to emphasize that when analyzing non-coaxial configurations, we did not take into account the distortion of skyrmion profiles by radial components H_ρ of the Pearl vortex field [23–25]. It should be also noted that the introduction to parameterizations (2) an additional parameter of the skyrmion helicity χ in the

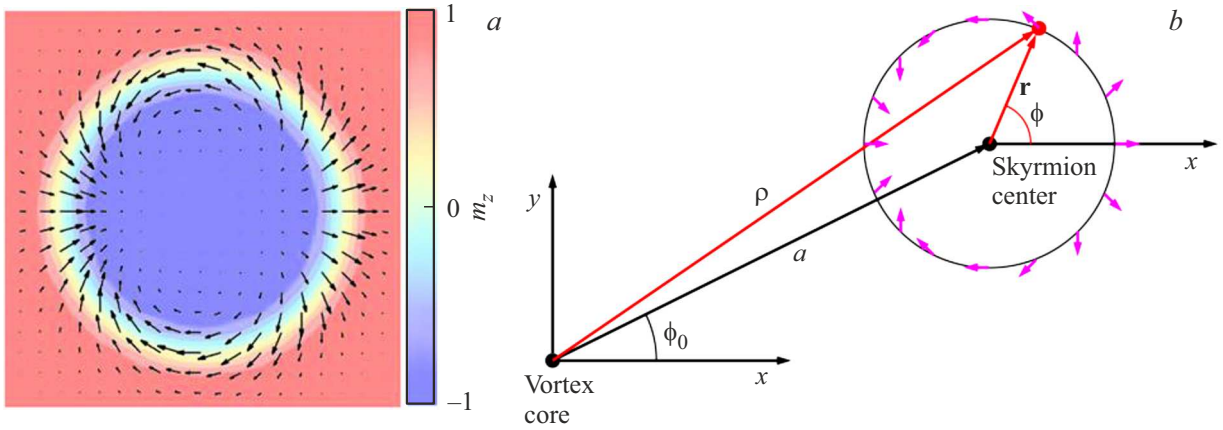

Figure 1. *a* — Spatial profile of a high-order magnetic skyrmion with $n = 2$. The arrows visualize the projection of the magnetization field $m(r)$ onto the film plane XoY. The colors correspond to the values of the magnetization projection in accordance with the color code shown on the right. *b* — Geometry of the relative position of the superconducting Pearl vortex and the HOMS with $n = 2$. The energy of a pair of PV and HOMS depends on the distance between their centers, and on the angle φ_0, which determines the mutual orientation of the centers.

presented consideration would lead to a renormalization of the angle φ_0, and therefore we chose $\chi = 0$ as the helicity origin point.

Assuming that the sizes of the skyrmion significantly exceed the lattice parameter $R, w \gg 1$, we can proceed to a continuous description of the functional (3). In this approximation, the excitation energy of the HOMS over the ferromagnetic state, $m_z \equiv 1$, is described by the functional $E[\mathbf{m}] = E_J + E_A + E_K + E_Z$ with the following energy contributions [19,21]:

$$E_J = \frac{\sqrt{3}S^2\mathcal{J}}{2}\int\limits_{\mathbb{R}_2}\sum_{\mu=x,y,z}(\nabla m_\mu)^2 ds,$$

$$E_A = \frac{2}{\sqrt{3}S^2\mathcal{A}}\int\limits_{\mathbb{R}_2}(1-m_z^2)ds, \qquad (6)$$

$$E_K = S^3\int\limits_{\mathbb{R}_2}\mathcal{K}(|\mathbf{r}-\mathbf{r}_0|)\cdot\left(\mathbf{m}\cdot\left[\frac{\partial\mathbf{m}}{\partial x}\times\frac{\partial\mathbf{m}}{\partial y}\right]\right)ds, \qquad (7)$$

$$E_Z = \frac{2Sg\mu_B}{\sqrt{3}}\int\limits_{\mathbb{R}_2}(H_z - \mathbf{H}(|\mathbf{r}-\mathbf{r}_0|)\cdot\mathbf{m})\cdot ds, \qquad (8)$$

where $|\mathbf{m}| = 1$, $\nabla = (\partial/\partial x, \partial/\partial y, 0)$, $ds = dx \wedge dy$, $r_0 = -(a\cdot\cos\varphi_0,\ a\cdot\sin\phi_0,\ 0)$.

The orbital effects of the PV stray fields are contained in the term E_K (8), which describes the scalar chiral interaction with an inhomogeneous core:

$$\mathcal{K}(|\mathbf{r}-\mathbf{r}_0|) = K\cdot\sin\left(\pi\Phi_\Delta(|\mathbf{r}-\mathbf{r}_0|)/\Phi_0\right). \qquad (9)$$

The coefficient $K_c = \frac{\sqrt{3}}{4}KS^3$ will be referred to as the amplitude of the SCI hereinafter. When modeling the HOMS with $n = 3, 4$, we will study both the lattice version of the functional (3) and the continuum version (6)–(8), in which the derivatives will be numerically approximated by a difference scheme on a square grid, the step of which is significantly less than R and w. At the same time, in the continuum limit, we assumed that $\Phi_\Delta = \sqrt{3}H_z(\mathbf{r})/4$.

Under conditions of the dominance of the exchange contribution, $E_J \gg E_K$, E_Z, E_A, there is a relationship between the radius and width of the HOMS domain wall, $R \sim nw$ [19]. The contributions, $E_J + E_A$, which do not depend on the relative position of the HOMS and PV, tend to collapse the skyrmion, i. e., they correspond to the optimal $R \to 0$. Taking into account the scalar chiral interaction E_K can, however, stabilize the finite-radius HOMS, for example, in the regime $K > 0$, $n > 1$ and $s_H = -1$. The latter corresponds to the case when the field of the Pearl vortex is counter-directed to the saturation magnetization of the film away from the skyrmion, which we will further consider. At the same time, taking into account small Zeeman corrections E_Z can significantly modify the optimal sizes of skyrmions.

Due to the dependence of the orbital and Zeeman terms (7)–(8) on the coordinate of the center of the PV $\mathbf{r}_0$, the energy functional of the HOMS depends on the polar variables r_0 and φ_0 (see Figure 1, *b*). In this case, the derivatives $\partial E_Z/\partial a$ and $\partial E_Z/\partial\phi_0$ are proportional, respectively, to the radial and azimuthal components of the resultant ponderomotor forces acting on the HOMS. As it was shown in Ref. [21], $n-1$ values of angle ϕ_0 are identified at $n > 1$:

$$\overline{\phi}_0^n = \left(1 + \frac{1+2m}{n-1}\right)\pi(\mathrm{mod}\,2\pi), \quad m \in \mathbb{Z} \qquad (11)$$

for which the forces act along radial directions, $\partial E/\partial\phi_0 = 0$, and the Zeeman contribution from the radial components of the Pearl field — directed along the film is negative, $E_Z^{(r)}(a) < 0$. Further, we will consider the behavior of the functional $E(a)$ along such directions.

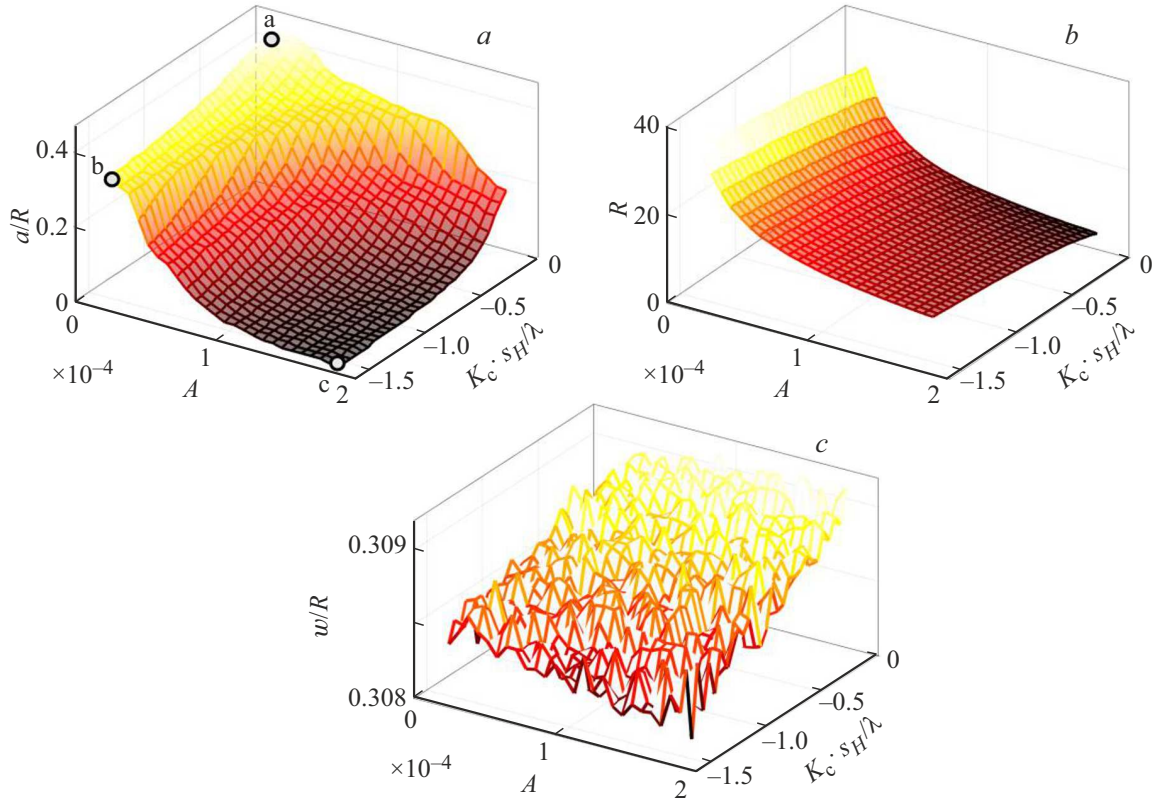

Figure 2. Dependences of a/R, R and w/R on the values of the anisotropy constants and scalar chiral interaction for the continuum model at $n = 3$.

The behavior of the functional $E(a)$ is determined both by the explicit dependence of the partial contributions on the parameter a and by the dependence of the radius of the skyrmion on the distance, $R = R(a)$. It was shown in Ref. [21] that although the latter dependence can lead to a significant redistribution of partial contributions from different interactions to the functional, certain trends in the behavior of the system can be understood from the analysis of only the explicit dependence $E(a)$. Such an analysis, partially contained in Refs. [19–21], shows the following features of the behavior of partial contributions in $E(a)$. The contribution from the Zeeman field components transverse to the film, $E_Z^{(z)}$, does not depend on the vorticity index n, and for small a increases as $E_Z^{(z)}|_{a \ll R} \sim -\beta_0 + \beta_z a^2$, where $\beta_z > 0$. The behavior of contributions related to the orbital effects E_K, as well as to the Zeeman effects $E_Z^{(r)}$ on the longitudinal Zeeman components of the Pearl vortex field already depends on n. So, in the case of $n \gg 1$, the behavior of $E_K(a)$ at small a is similar to the behavior of $E_Z^{(z)}$. Thus, the contributions to the functionality of E_K and $E_Z^{(z)}$ show a tendency to form a coaxial bound pair of PV−HOMS. At the same time, the negative contribution $E_Z^{(r)} \propto a^{n-1}$ from the longitudinal components of the field is expected to be suppressed at $n \gg 1$. Thus, for HOMS with large $|Q|$, the possibility of forming coaxial bound pairs with PV is expected. Numerical calculations show that the case $n \gg 1$ actually occurs for $n \geq 5$.

For the HOMS with $1 < n < 5$, the case $n = 2$ is singled out separately, in which $E_Z^{(r)}|_{a \ll R} \sim -C \cdot a$ with a coefficient $C > 0$. Considering the above about the behavior of $E_K(a)$ and $E_Z^{(z)}(a)$, the latter means that the energy of the bound pair PV−HOMS with $n = 2$ decreases with increasing a, and therefore the coaxial configurations are not implemented. It is important to note here that the degree of dependence of $E_K(a) - E_K(0) \propto a^{\alpha_K}$ on $\alpha_K = 2$, typical for $n \gg 1$, may differ for $n = 2$. However, numerical calculations have shown that α_K does not turn out to be less than or equal to one, and the conclusion about the absence of coaxial pairs PV−HOMS with $n = 2$ is not violated. When $n = 3$, 4, the competition of effects from the longitudinal and transverse components of the Pearl field becomes more complicated, and it is difficult to obtain analytical estimates for partial contributions to the functional, even ignoring the dependencies $R(a)$ and $w(a)$. Therefore, the further analysis of the HOMS with $n = 3$, 4 was conducted numerically.

3. Bound states of PV−HOMS with $n = 3$, 4

We performed numerical calculations of the continuum version of the functional (6)−(8) on a square grid to identify the main trends in the behavior of a bound pair PV−HOMS with $n = 3$. The main analysis was carried out under the

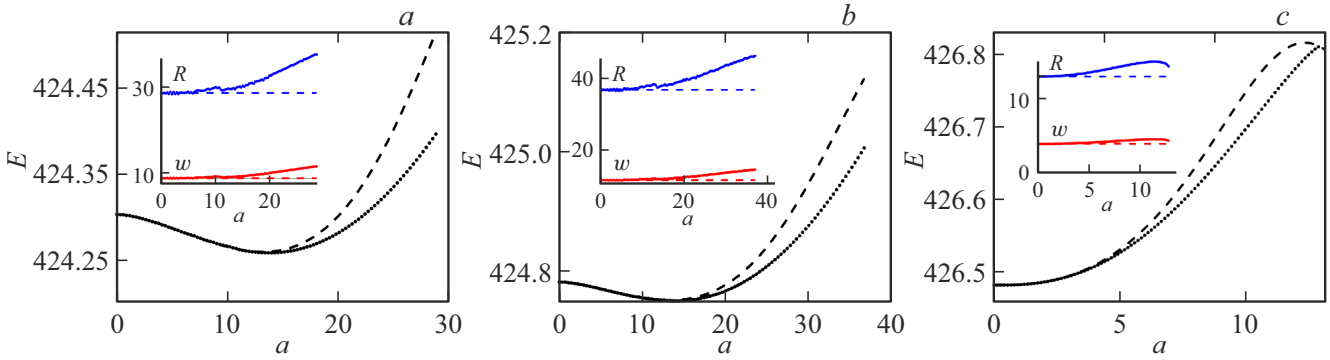

Figure 3. Dependences of the skyrmion energy on the displacement value for parameters corresponding to the three points *a, b* and *c* in Figure 2, *a*. The optimization of the HOMS size was also carried out when calculating dotted lines concurrently with finding the energy as a function a. The dashed lines are calculated at fixed values of R and w, obtained at $a = 0$.

assumption that the optimal sizes of the skyrmion, $R(a)$ and $w(a)$, can change with distance from the Pearl vortex: the minimization of the functional $E(R, w, a)$ was carried out for each defined value a. However, for completeness, calculations were also carried out under the assumption that the optimal sizes of the HOMS are determined by the functional in the coaxial configuration, and do not change with an increase of the distance from PV. At the same time, in the continuum approximation, it has always been assumed that the grid step is $\delta \ll R, w$.

As mentioned above, the regime $E_J \gg E_K$, E_Z, E_A sets the relationship $R \sim nw$, clearly demonstrated in Figure 2, *c* for the case $n = 3$. In addition, since the tendency for the shift of the HOMS is formed due to the interaction of the radial components of the PV with the skyrmion domain wall in the vicinity of the radius R, it is obvious that the nonzero optimal values of the displacement parameter will be proportional to the radius of the skyrmion $a \propto R/2$. Thus, to analyze the degree of coaxiality of the bound pairs of PV–HOMS, as well as the sizes of the HOMS, it is sufficient to analyze the values of a/R and R, respectively.

The dependences calculated in the continuum approximation, a/R and R for HOMS with $n = 3$ on the energy parameters of single-ion anisotropy A and scalar chiral interaction K_c are shown in Figure 2. It can be seen that the size of the skyrmion decreases rapidly with increasing anisotropy, $R \propto A^{-\alpha}$, and increases slowly with increasing intensity of the scalar chiral interaction, $R \propto K_c^{\beta}$. It can be seen that the eccentric configurations with $a/R \propto 0.5$ correspond to skyrmions of large radii, $R \gg 1$, whereas with a decrease in the size of the skyrmions, there is a tendency to form coaxial configurations. The latter can be determined by the condition that the displacement parameter a becomes smaller than the grid step.

From the consideration of the dependencies in Figure 2, *a* and 2, *b*, it can be seen that in the continuum approximation, the formation of coaxial coupled pairs of PV–HOMS with $n = 3$ is possible, however, this occurs when the skyrmion sizes $R \sim 10$, $w \sim 3$, for which the continuum approximation turns out to be inapplicable. To clearly demonstrate this statement, Figure 3 shows the dependences of the energy of the HOMS E on the distance a for three different sets of parameters corresponding to the points *a, b* and *c* in Figure 2, *a*. It can be seen that the non-coaxial configurations *a* and *b* correspond to sufficiently large HOMS, and the coaxial case *c* corresponds to skyrmions with sizes that are insufficiently small for a continuous description. Thus, the calculations given in the continuum approximation allow seeing the tendency of the HOMS with $n = 3$ to form a coaxial coupled pair with the PV, but do not guarantee its formation.

For a more detailed study of the possibility of the formation of coaxial coupled pairs, we calculated the same dependences a/R, R and w/R, but within the framework of the lattice functional (3). The calculation results in the narrower range of the parameters A and K_c are shown in Figure 4. In this case, the ratio $R \approx nw$ is still fulfilled, however, there are critical parameter lines at which the HOMS with $n = 3$ collapse without reaching a coaxial state due to the small size and discreteness of the lattice.

Thus, although in the case of bound pairs of PV–HOMS with $n = 3$ the continuum limit allows for a coaxial pairs, it corresponds to skyrmions of such small sizes that the actual ones are unstable when taking into account the effects of lattice discreteness. As a result, for the hierarchy of energy contributions we are studying $E_J \gg E_K$, E_Z, E_A, it can be argued that in the case of $n = 3$ only non-coaxial bound pairs are realized, as in the case of $n = 2$.

Next, we examined the behavior of the pairs of PV–HOMS with $n = 4$. The results of calculations of the dependence $E(a)$, similar to those shown in Figure 3, are presented in Figure 5 for two sets of system parameters. From their consideration, it can be seen that in the case of $n = 4$, coaxial bound states are implemented. We observed such a configuration for all the parameters under consideration, even with small values of the three-spin interaction. The explanation for this effect is a slower increase in the dependence of the negative contribution to

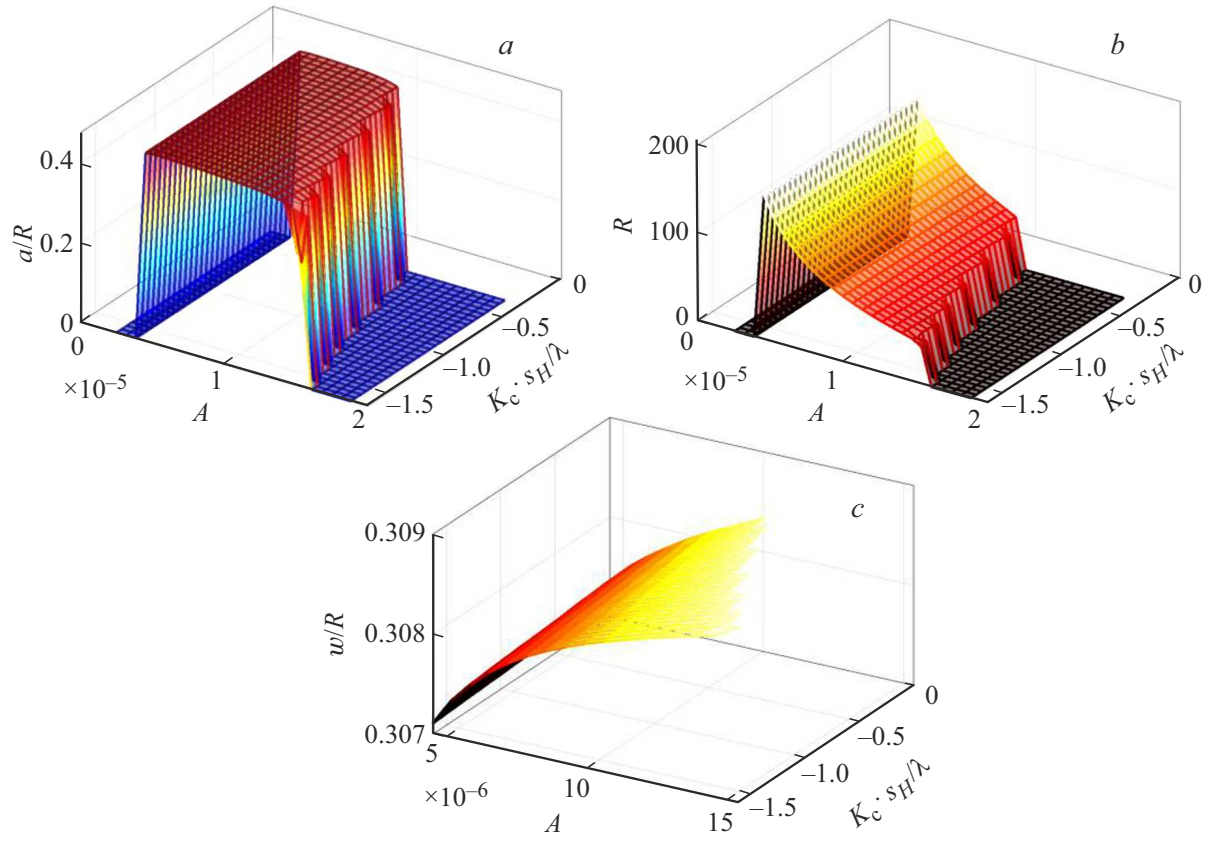

Figure 4. Dependences of a/R, R and w/R on the values of anisotropy constants and scalar chiral interaction on a discrete triangular lattice.

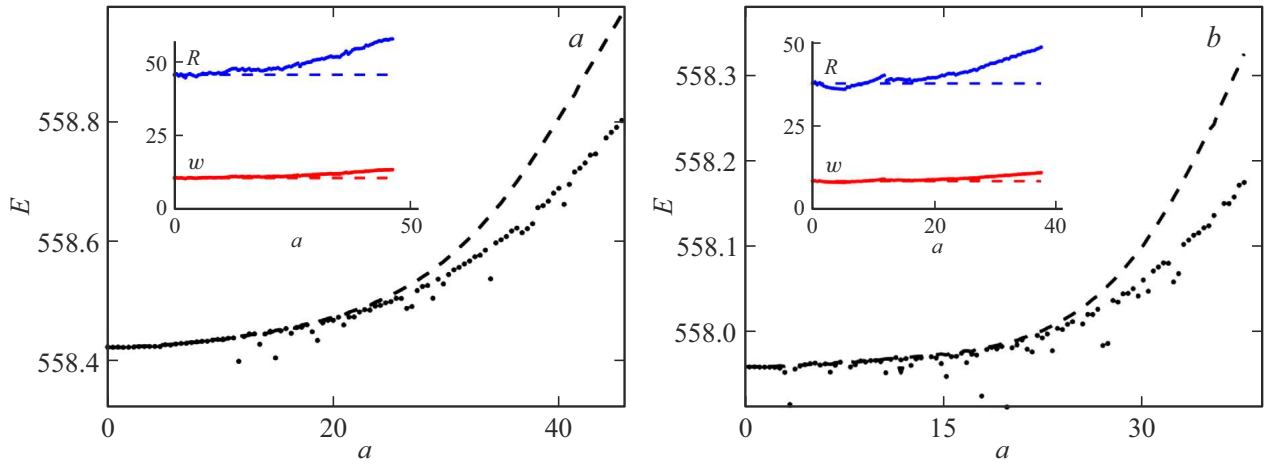

Figure 5. Dependences of the skyrmion energy on the displacement value for $n = 4$. The dots correspond to the energy minimization at a given a by the size of the skyrmion R, w, dashed line corresponds to the energy dependence at fixed R, w obtained for $a = 0$.

the Zeeman energy on the radial component of the field on the magnitude of the displacement a compared to the positive growth from terms describing the perpendicular component already at $n = 4$. At the same time, with an increase in the intensity of the scalar chiral interaction, the severity of the minimum dependence $E(a)$ at $a = 0$ increases. Considering the above, the behavior of dependencies $E_Z^{(r)}(a)$, $E_Z^{(z)}(a)$ and $E_K(a)$ is expected to implement coaxial pairs for $n \geq 4$.

4. Conclusion

The possibility of stabilization in thin superconductor/chiral magnet heterostructures of coaxial pairs of a

Pearl vortex and high-order magnetic skyrmions with small topological charges n was studied in this paper. The main mechanism of stabilization was considered to be the competition of exchange interaction, easy-axial single-ion anisotropy, as well as the orbital and Zeeman effects of vortex scattering fields. At the same time, we considered the regime of dominance of the exchange coupling in magnetic films, in comparison with other magnetic interactions. In this regime, the characteristic dimensions of skyrmions — their radius and the width of the domain wall — turn out to be related to the topological charge $R \approx nw$. Candidates for the considered system are layered strongly correlated compounds in which magnetic interactions occur due to indirect exchange, for example, transition metals $3d$ and rare earth metals $4f$ [40].

The described formulation of the study is a natural continuation of Ref. [21], which focused on the HOMS with $n = 2$ and $n \gg 1$. Thus, it follows from the analysis that for the simplest HOMS with $n = 2$ eccentric coupled pairs are always realized, whereas for HOMS with $n \gg 1$ it is possible, and even expected, the formation of coaxial pairs, the analytical theory for which was developed in Refs. [19,20]. In the intermediate case, the competition of the effects of the longitudinal and transverse components of the Pearl vortex field on the HOMS becomes more complicated, and crossovers between different regimes can occur with minor changes in the energy parameters of the system. Therefore, we studied the analysis of the possibilities of implementing coaxial bound pairs for HOMS with $n = 3, 4$ numerically.

We have demonstrated that in the case of $n = 3$ and $n = 4$, skyrmions can also stabilize in the fields of the Pearl vortex due to orbital effects. In the case with $n = 3$, although there is a tendency to switch to the coaxial regime with an increase in the anisotropy parameters and the magnitude of the three-spin interaction, however, this occurs at parameters at which the HOMS can no longer be stable due to its small size. Therefore, an eccentric coupled pair of HOMS with a Pearl vortex is actually realized for $n = 3$ as in the case of $n = 2$. In the case of the HOMS with $n = 4$, a coaxial configuration with a Pearl vortex is implemented, and it is expected that this situation will persist for $n \geq 4$.

In conclusion, we note that this study is predictive in nature, since there are currently no data from numerical and physical experiments to verify our results. Thus, in recent experimental studies, high-order skyrmions with $|Q| > 1$ [7] and coupled pairs of magnetic skyrmion with $|Q| = 1$ — superconducting vortex(antivortex) have been studied separately [41,42]. As far as we know, the coupled pairs of the Pearl vortex−HOMS with $|Q| > 1$ have not been experimentally studied. The lack of numerical experimental data is due to the fact that standard magnetic modeling packages (for example, OOMMF [34]) are not optimized for calculating the scalar chiral interaction.

Acknowledgments

The authors would like to thank I.S. Burmistrov, S.S. Apostolov, and E.S. Andriakhina for important discussions.

Funding

The work was performed within the framework of the state tasks FWES-2024-0002 „Studies of ordered states in condensed matter: synthesis of new materials, experiment and theory“ (IF SB RAS) and FFWR-2024-0017 „Transport in disordered systems: from nanostructures to a turbulent atmosphere“ (Landau Institute for Theoretical Physics of RAS). SHMS would like to thank the Foundation for the Development of Theoretical Physics and Mathematics „BASIS“ for its individual support.

Conflict of interest

The authors declare that they have no conflict of interest.

References

[1] A.A. Belavin, A.M. Polyakov. Pisma v ZhETF **22**, 503 (1975). (in Russian).
[2] F.N. Rybakov, O. Eriksson, N.S. Kiselev. arXiv:2412.17641v1 (2024).
[3] S.S.P. Parkin, M. Hayashi, L. Thomas. Science **320**, 190−194 (2008).
[4] S.S.P. Parkin, S.-H. Yang. Nat. Nanotechnol. **10**, 195−198 (2015).
[5] C. Psaroudaki, E. Peraticos, C. Panagopoulos. Appl. Phys. Lett. **123**, 260501 (2023).
[6] L. Rózsa, K. Palotás, A. Deák, E. Simon, R. Yanes, L. Udvardi, L. Szunyogh, U. Nowak. Phys. Rev. B **95**, 094423 (2017).
[7] M. Hassan, S. Koraltan, A. Ullrich, F. Bruckner, R.O. Serha, Kh.V. Levchenko, G. Varvaro, N.S. Kiselev, M. Heigl, C. Abert, D. Suess, M. Albrecht. Nat. Phys. **20**, 615–622 (2024).
[8] F. Rybakov, N. Kiselev. Phys. Rev. B **99**, 064437 (2019).
[9] V.M. Kuchkin, B. Barton-Singer, F.N. Rybakov, S. Blugel, B.J. Schroers, R.N. Kiselev. Phys. Rev. B **102**, 144422 (2020).
[10] J. Tang, Y. Wu, W. Wang, L. Kong, B. Lv, W. Wei, J. Zang, M. Tian, H.U. Du. Nat. Nanotechnol. **16**, 1086−1091 (2021).
[11] L. Yang, A. Savchenko, F. Zheng, N.S. Kiselev, F.N. Rybakov, X. Han, S. Blügel, R.E. Dunin-Borkowski. Adv. Mater. **36**, 2403274 (2024).
[12] B. Seng, D. Schonke, J. Yeste, R.M. Reeve, N. Kerber, D. Lacour, J.-L. Bello, N. Bergeard, F. Kammerbauer, M. Bhukta, T. Ferté, Ch. Boeglin, F. Radu, R. Abrudan, T. Kachel, S. Mangin, M. Hehn, M. Kläu. Adv. Funct. Mater. **31**, 2102307 (2021).
[13] D.S. Kathyat, P. Sengupta. Phys. Rev. B **110**, 144409 (2024).
[14] A.N. Bogdanov, D.A. Yablonsky. Sov. Phys. JETP **95**, 178 (1989).
[15] M.A. Kuznetsov, A.A. Fraerman. ZhETF **164**, 514−525 (2023). (in Russian).
[16] A. Leonov, M. Mostovoy. Nat. Commun. **6**, 8275 (2015).

[17] R. Ozawa, S. Hayami, Y. Motome. Phys. Rev. Lett. **118**, 147205 (2017).
[18] K.L. Metlov. Phys. Rev. Lett. **105**, 107201 (2010).
[19] M.S. Shustin, V.A. Stepanenko, D.M. Dzebisashvili. Phys. Rev. B. **107**, 195428 (2023).
[20] M.S. Shustin, D.M. Dzebisashvili, V.A. Stepanenko. FTT, **65**, 1021 (2023). (in Russian).
[21] A.D. Fedoseev, M.S. Shustin, D.M. Dzebisashvili. Pisma v ZhETF **120**, 539 (2024). (in Russian).
[22] E.S. Andriyakhina, I.S. Burmistrov. Phys. Rev. B **103**, 174519 (2021).
[23] E.S. Andriakhina, S. Apostoloff, I.S. Burmistrov. Pisma v ZhETF **116**, 801 (2022). (in Russian).
[24] S.S. Apostoloff, E.S. Andriyakhina, P.A. Vorobyev, O.A. Tretiakov, I.S. Burmistrov. Phys. Rev. B **107**, L220409 (2023).
[25] S.S. Apostoloff, E.S. Andriyakhina, I.S. Burmistrov. Phys. Rev. B **109**, 104406 (2024).
[26] G. Yang, P. Stano, J. Klinovaja, D. Loss. Phys. Rev. B **93**, 224505 (2016).
[27] A.P. Petrovic, M. Raju, X.Y. Tee, A. Louat, I. Maggio-Aprile, R.M. Menezes, M.J. Wyszyński, N.K. Duong, M. Reznikov. Phys. Rev. Lett. **126**, 117205 (2021).
[28] E. Andriyakhina, I. Burmistrov. Phys. Rev. B **103**, *17*, 174519 (2021).
[29] U. Gungordu, A.A. Kovalev. J. Appl. Phys. **132**, 041101 (2022).
[30] J. Nothhelfer, S.A. Díaz, S. Kessler, T. Meng, M. Rizzi, K.M.D. Hals, K. Everschor-Sitt. Phys. Rev. B **105**, 224509 (2022).
[31] S.T. Konakanchi, J.I. Väyrynen, Y.P. Chen, P. Upadhyaya, L.P. Rokhinson. Phys. Rev. Res. **5**, 033109 (2023).
[32] D. Sen, R. Chitra. Phys. Rev. B **51**, 1922 (1995).
[33] O.I. Motrunich. Phys. Rev. B **73**, 155115 (2006).
[34] A.O. Leonov, T.L. Monchesky, N. Romming, A. Kubetzka, A.N. Bogdanov, R. Wiesendanger. New J. Phys. **18**, 065003 (2016).
[35] R.M. Menezes, J.F.S. Neto, C.C. de Souza Silva, M.V. Milosevic. Phys. Rev. B **100**, 014431 (2019).
[36] J. Pearl. Appl. Phys. Lett. **5**, 65 (1964).
[37] A.A. Abrikosov. Fundamentals of the Theory of Metals. North-Holland, Amsterdam (1988).
[38] G. Carneiro, E.H. Brandt. Phys. Rev. B **61**, 6370 (2000).
[39] X. Wang, H. Yuan, M.X. Wang. Commun. Phys. **1**, 1 (2018)
[40] V.Yu. Irkhin, Yu.P. Irkhin. Elektronnaya strultura, korrelyatsionnye effekty i fizicheskie svoistva *d*- i *f*-perekhodnykh metallov i ikh soedineniy i ikh soedineniy. RKhD, M. (2008). p. 476 (in Russian).
[41] Y. Xie, A. Qian, B. He, Y.-B. Wu, Sh. Wang, B. Xu, G. Yu, X. Han, X.G. Qiu. Phys. Rev. Lett **133**, 166706 (2024).
[42] M. Beg, M. Lang, H. Fangohr. IEEE Trans. Magn. 58, **1** (2022).

Translated by A.Akhtyamov